Geomechanics and Engineering, *Vol. 43, No. 4 (2025) 301-313*
https://doi.org/10.12989/gae.2025.43.4.301

Investigation of torque-capacity correlations and new formulas for torque factor based on axially compression-loaded helical piles

Yakup Türedi*[1], Muhammet Dingil[1], Buse Emirler[2], Murat Örnek[1] and Abdulazim Yıldız[2]

[1]*Department of Civil Engineering, Iskenderun Technical University, Hatay 31200, Türkiye*
[2]*Department of Civil Engineering, Cukurova University, Adana 01250, Türkiye*

(*Received July 26, 2024, Revised November 4, 2025, Accepted November 7, 2025*)

Abstract. The empirical torque factor (K_t) is a critical parameter for predicting the ultimate compressive capacity of helical piles from installation torque. However, current K_t values may be limited by the derivation from combined axial loads, an exclusive reliance on shaft diameter, and the scarcity of adequate and diverse test data. This study introduces more robust and reliable K_t correlations by developing models derived solely from compression load tests that integrate both the helical pile's shaft diameter (d) and embedded area (E_A). A total of 20 model helical piles were installed and loaded axially compression in loose and dense sand to investigate installation torque-ultimate capacity behavior. The depth-torque profiles and load-displacement curves were obtained from model laboratory tests for various helix diameters, numbers, and spacing. Furthermore, installation torques (T) varying from torque reading methods (max., end pile, and average) were examined, and K_t values were showed variations of approximately 10% with different T values. These results were synthesized with a comprehensive database compiled from literature to create two extensive datasets correlating K_t with both shaft diameter and embedded area. The proposed novel equations for calculating K_t demonstrate a strong statistical fit, with high coefficients of determination (R^2) of 0.94 and 0.90 for the d-based and E_A-based correlations, respectively. These validated models offer a significant improvement over existing methods, providing a sounder framework for the design of compression-loaded helical piles.

Keywords: compression load; dense sand; embedded area; helical pile; installation torque; loose sand; torque factor

1. Introduction

Helical piles are a type of pile that can support compression, uplift, dynamic and lateral loading, easy to manufacture and simple to implement, can be installed by applying torque it towards the soil in an inclined or perpendicular manner with the help of a drive head. By virtue of their low-impact installation, which generates minimal noise and vibration, coupled with their inherent reusability, helical piles represent a prominent sustainable foundation alternative (Kim *et al.* 2023, Ebadi-Jamkhaneh *et al.* 2025). There are one or more steel helix-plates welded to the pile shaft and can be installed easily into the soil by applying torque to the upper end of the shaft, in helical piles (Fateh *et al.* 2018, Kim *et al.* 2022). During the installation of helical piles, varying torque resistance depending on the depth can be monitored (Aoki *et al.* 2007). Helical piles, one of the deep foundation types, are widely used in many areas of geotechnical engineering thanks to their resistance to many different types of loads (compression, lateral, etc.) and can be easily applied on many different types of soils (swampy, frost-sensitive, poorly, etc.).

In helical piles, loading tests are generally performed in determining the ultimate bearing capacity of the piles. The ultimate capacity can be stated according to various methods on the obtained load-displacement curves. There are major studies in the literature on determining the behavior of helical piles under compression loading and their ultimate bearing capacity (Sakr 2009, Sprince and Pakrastinsh 2010, Elsherbiny and El Naggar 2013, Salhi *et al.* 2013, Gavin *et al.* 2014, Lutenegger and Tsuha 2015, Lanyi-Bennett and Deng 2019a, Türedi and Örnek 2020, Bak *et al.* 2021,).

On the other hand, installation torque values can be used as an alternative to the compression loading test to find the bearing capacity of helical piles. Hence, installation torque for helical piles is an important parameter in terms of application, and in the literature, the relation between installation torque and ultimate bearing capacity is interpreted using of empirical torque factor. Accordingly, the ultimate capacity of helical piles can be determined from the load-displacement curves or by multiplying the installation torque with an empirical torque factor.

The ultimate capacity of helical piles is achieved through a constant torque factor associated with the installation torque, usually based on the shaft diameter. Many studies including field and laboratory tests have been carried out to evaluate the ultimate capacity-torque correlation factor (K_t) under different parameters (such as different shaft and helix diameters, soil conditions). There is an increasing number of experimental and theoretical studies offering different approaches to determine the installation torque-pile capacity relationship. Souissi (2019) presented an approach based on the ratio of effective pile diameter to final installation torque (D/T) instead of shaft

*Corresponding author, Assistant Professor
E-mail: yakup.turedi@iste.edu.tr

ISSN: 2005-307X (Print), 2092-6219 (Online)

diameter when determining the K_t torque factor for the pile capacity- torque relationship. Harnish and El Naggar (2017) introduced the torque factor approach based on the total surface area of embedded helical piles.

One of the most important features of helical piles is that an empirical relationship can be established between these installation torques and the ultimate soil capacity by reading the torque values applied during their installation. This method is similar to determining pile driving capacity and pile capacity (Souissi 2020). It is recognized that the installation torque can be used to estimate the axial capacity of the helical pile for both tensile and compression loads. Generally, the torque value changes depending on the soil conditions and the geometric properties of the helical pile. The empirical relationship of the axial capacity of helical piles depending on the installation torque is defined by the torque factor given in Eq. (1) (Hoyt and Clemence 1989, CFEM 2006, Perko 2009).

$$Q_u = K_t T \quad (1)$$

where Q_u= ultimate helical pile capacity, K_t= empirical torque factor, T= installation torque value.

The relationship between helical pile capacity and torque was first described in the literature by Hoyt and Clemence (1989), and this relationship is considered a milestone in the helical pile industry (Perko 2009). It was stated by Hoyt and Clemence (1989) that the empirical torque factor (K_t) is a constant that depends only on the shaft diameter, independent of the helical plate number and helix diameter, loading path and soil conditions. The torque factor (K_t) value was taken as 33 m^{-1} if the shaft diameter is less than 89 mm, 23 m^{-1} if the shaft diameter is equal to 89 mm, and 9.8 m^{-1} if the shaft diameter is 219 mm reported by Hoyt and Clemence (1989).

In the literature, K_t values were mainly based on the results of tensile tests for small diameter piles (less than 90 mm), and therefore, Sakr (2015) states that the axial capacities of especially large diameter helical piles or helical piles under compression cannot be fully estimated. In the study conducted by Sakr (2015), the interaction between the installation torque and axial capacity of helical piles in cohesionless soils was investigated. Accordingly, separate formulations have been proposed, containing K_C (compression torque factor) for the compression condition and K_t (tensile torque factor) for the tensile state. Expressed as the ratio between axial compression and torque (Sakr 2015), the K_C value can be calculated as follows (Eq. (2)).

$$K_c = \frac{Q_c}{T} = \frac{Q_s + \sum_{j=1}^{N} Q_{hj}}{\sum_{j=1}^{N}\sum_{i=1}^{i=8} T_{ij}} = \frac{\pi d L q_s + \sum_{j=1}^{N} A_{hj}(\gamma D_{hj} N_q + 0.5\gamma D_j N_\gamma)}{\sum_{j=1}^{N}\sum_{i=1}^{i=8} T_{ij}} \quad (2)$$

where d = shaft diameter, L = length of pile shaft, and q_s = average unit shaft friction of soil, A_{hj} = helix area; γ = soil unit weight, D_{hj} = helical plate depth, D_j = helical plate diameter, N_q ve N_γ = bearing capacity factors for local shear conditions, N = number of helices, T_{1j} = torsional moment acting on pile shaft (kNm), and T_{2j} to T_{8j} = torsional moment components acting on a helix j (kNm). The bearing capacity factors, N_q and N_γ, can be calculated using Meyerhof's breakout theory and Vesić's bearing resistance model (Asgari *et al.* 2025).

An empirical relationship between K_t and effective shaft diameter (d_{eff}) has been proposed by Perko (2009) based on the exponential regression analysis of more than 300 loading tests for both compression and tension conditions (Harnish 2015). Based on this empirical torque correlation relationship, a torque factor determination equation based on shaft diameter proposed by Perko (2009) is given in Eq. (3).

$$K_T = \frac{\lambda_k}{d_{eff}^{0.92}} \quad (3)$$

where λ_k = curve fitting factor (1433 $mm^{0.92}$), d_{eff} = effective shaft diameter (mm).

A review of the literature on the torque correlation coefficient reveals that existing studies present several limitations. The proposed torque factors are often derived from a combination of compression and tension tests, based on pile tests of a specific scale, correlated solely with the shaft diameter, and suffer from a scarcity of data for alternative correlation models. The unique contribution and novelty of this study lie in the development of torque correlation factors that address these gaps. Specifically, the factors proposed in this paper are: (1) derived exclusively from compression load test results of various-scaled helical piles, and (2) correlated with both the shaft diameter and the embedded area. These correlations are represented across a wide spectrum and validated by a high coefficient of determination offering a more robust and broadly applicable model.

This study investigates the torque-capacity relationships of helical piles through a series of laboratory model tests, systematically varying helix diameter, number, and spacing under dense and loose sand conditions. Furthermore, it has revealed the influence of various installation torque assessment methods on the torque correlation factor, as evidenced by the torque-depth profiles. The main objective of this paper is to develop highly correlated and generalized torque factor formulations that surpass single-scale derivations, by strategically integrating findings from model tests into a comprehensive heterogeneous database of laboratory and field results presented in the literature, thereby addressing complex scaling challenges. By analyzing this extensive dataset, two novel mathematical equations are proposed that establish a highly correlated relationship with shaft diameter (d) and present a more comprehensive physical model based on total embedded area (E_A). These equations, whose robustness was confirmed using an independent validation subset, provide an empirically validated framework for predicting ultimate compressive capacity from installation torque, effectively bridging the gap between model-scale behavior and field-scale design.

2. Experimental work

The model load tests were conducted Iskenderun Technical University, Geotechnical Laboratory of Civil Engineering Department, Hatay, Türkiye. The model tests were performed in a rectangular test tank 1.5 m x 1.2 m in plan dimension and 1.0 m in depth. The frame of the test

tank is made of 8 mm thick steel profile and the front and left side the box surfaces are made of 10 mm thick glass panel. The other side surfaces are made of 3 mm thick metal sheet panel material. To mitigate adverse boundary effects, the experimental setup adhered to established guidelines summarized by Sahil *et al.* (2025). The literature recommends that the distance between the pile and the side walls should be 3 to 8 times the pile tip diameter (Kishida 1963), while the clearance between the pile tip and the tank base should be 3.5 to 5.5 times this diameter (Yu and Yang 2012). In the present study, the clearances around the pile shaft and beneath its tip were approximately 12 and 4 times the pile tip diameter, respectively. These dimensions are consistent with the recommended ranges, thereby ensuring the model test results were not compromised by boundary interference.

2.1 Soil properties

The sand soil used in the experimental studies were obtained from the sand quarry. It was subjected to sieve analysis according to ASTM D2487-11 (2011). Soil class is determined as SP (poorly graded sand) according to the Unified Soil Classification System (USCS). The sand with an effective size of 0.261 mm, uniformity coefficient of 2.973, coefficient of curvature of 0.961 and a particle size less than 2 mm.

In the model tests, the relative densities for loose (D_r=30%) and dense (D_r=80%) sand were determined in accordance with ASTM D4253-16e1 (2016) and ASTM D4254-16 (2016). To serve as a reference during the preparation of the sand beds, the glass surface of the test tank was marked with 5 cm increments. The loose soil conditions were prepared using the raining technique. This technique fundamentally involves the pluviation of sand grains from a predetermined height, typically utilizing one or more sieves to ensure a steady and uniform deposition (Yang *et al.* 2024). For this purpose, the loose sand beds were formed by releasing sand from a height of 5 cm through a custom-built sieve with a 5x5 mm mesh, which was movable within the test container. The dense sand medium was achieved by weighing sand samples to reach a target post-compaction unit weight of 16.48 kN/m³, placing them into the test container, and then compacting them with a vibratory compactor to a relative density of D_r=80% (ASTM D2167-15 2015). A consistent and meticulous methodology was followed for each step of the bed preparation process to guarantee the reliability and repeatability of the experimental outcomes. The soil properties are presented in Table 1.

Table 1 Soil properties of dense and loose sand

Parameter	Dense	Loose	Unit
D_r	80	30	%
γ_k	1.681	1.552	gr/cm^3
ϕ	43	30	°

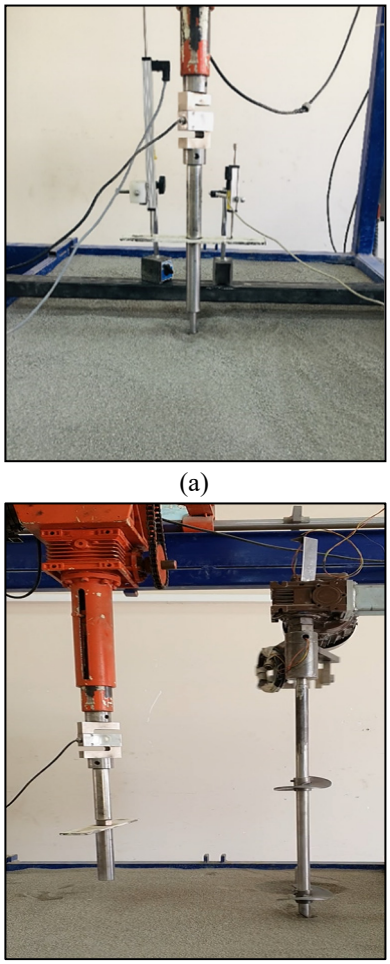

(a) (b)

Fig. 1 (a) Test setup and (b) helical pile installation

2.2 Test setup

In the study, failure mechanisms and torque variations of model helical piles of different parameters subjected to axial compression load were investigated. During the installation of the helical piles, torque values were recorded instantaneously throughout the depth, and torque measurement system is placed between the torque motor and the helical pile (Fig. 1). The load was vertically applied to head of the model helical pile by an electrically operated mechanical jack system. The helical pile installation assembly consists of an electric motor fixed to the test tank during experimental studies and used to fix the helical piles to the soil by rotating them. The experimental setup and torque reading system is given in Fig. 2 as a schematic view.

The model helical piles were fabricated from straight, open-ended steel shafts (d = 22 mm) with a wall thickness (t) of 2.5 mm. These shafts were designed to accommodate helical plates with varying parameters, including the number of helices (N), helix spacing (s), and helix diameter (D), which were detailed in Table 2 and shown schematically in Fig. 3. The pitch of each helix was defined as 0.3 times the helix diameter (0.3D).

Table 2 Model test details

Test ID	Relative Density, D_r (%)	Pile Length, L (mm)	Helix Diameter, D (mm)	Helix Number, N	Helix Spacing/Helix Diameter, s/D
LCDT-2	80	600	60	1	-
LCDT-3			80	1	-
LCDT-4			100	1	-
LCDT-5			120	1	-
LCDT-7			100	2	1.5
LCDT-8			100	2	2.0
LCDT-9			100	2	2.5
LCDT-10			100	2	3.0
LCDT-11			100	3	1.5
LCDT-12			100	3	2.0
LCLT-2	30	600	60	1	-
LCLT-3			80	1	-
LCLT-4			100	1	-
LCLT-5			120	1	-
LCLT-7			100	2	1.5
LCLT-8			100	2	2.0
LCLT-9			100	2	2.5
LCLT-10			100	2	3.0
LCLT-11			100	3	1.5
LCLT-12			100	3	2.0

LCDT: Laboratory-Compression-Dense-Test | LCLT: Laboratory-Compression-Loose-Test

1- reaction beam 2- mechanical beam 3- load cell 4- lvdt 5- helical pile 6- test tank 7- steel plate 8- glass plate 9- steel profile 10-torque motor 11- torque control unit 12- torque reading system 13- lvdt (depth readings for torque measurement)

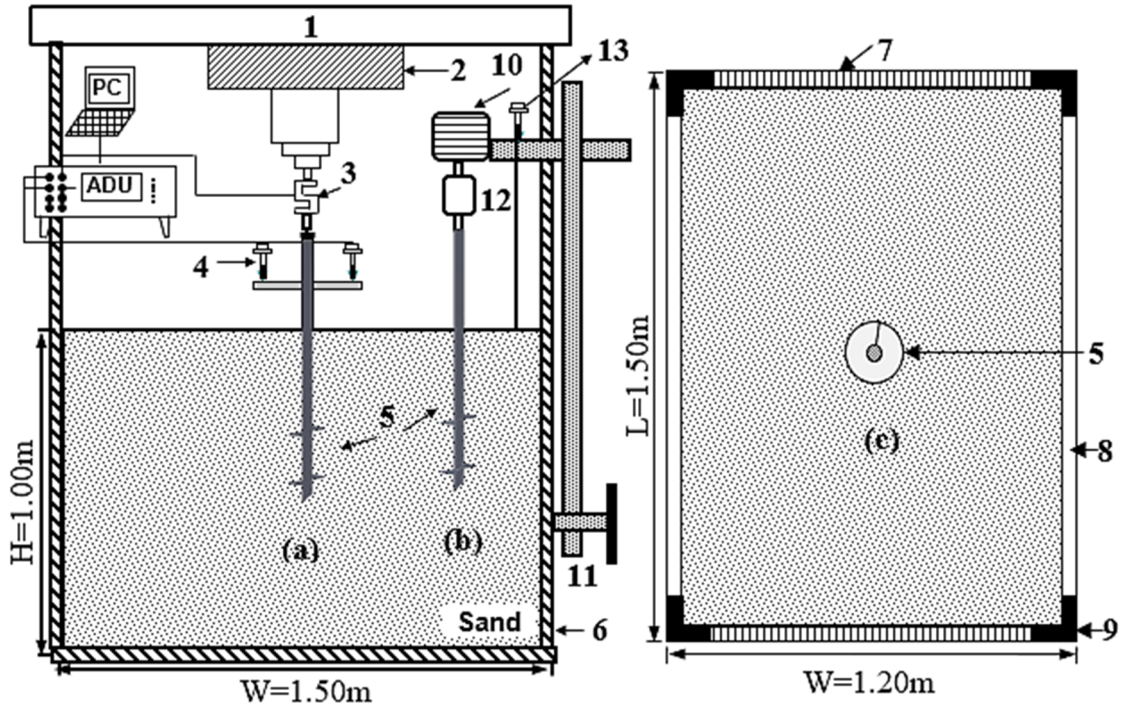

Fig. 2 The illustration of the loading and installation system of model helical piles (a) installation equipment, (b) pile test setup and (c) plan view

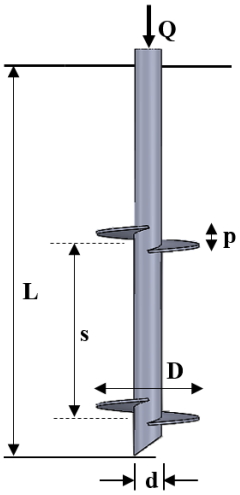

Fig. 3 Schematic view of helical piles geometry

For loose and dense soil conditions, a total of 20 model tests were carried out model helical piles under compression load. To ensure the repeatability and consistency of the experimental outcomes, the model tests were repeated under both dense and loose soil conditions, and these repeated tests yielded highly consistent results. In this study, repeated tests were specifically conducted for model helical piles with the largest helix diameter and multiple helical plates at various s/D ratios. Ultimately, when comparing the repeated tests to the initial ones, the load-displacement curves and torque-depth profiles were observed to be closely aligned and consistent.

3. Results and discussion

3.1 Pile installation torque profiles

In the model tests, during the installation of the model helical piles on the soil, the installation torques were taken per second through installation depth. Depth-torque profiles of model helical piles were presented in Fig. 4 for different test conditions.

The change in the helix diameter has significantly increased the torque values for both dense and loose soil. As seen that there is an increase of 5-10 times in torque values on dense sand soil compared to loose sand soil, depending on the increase in the diameter of the helix. When the effect of helix spacing/helix diameter was examined, it was determined that the installation torques were found values very close to each other in the case of the double helix at especially dense sand conditions.

3.2 Installation torque measurement

In the literature, installation torque used when determining pile bearing capacity depending on torque values can be different from each other. Livneh and El Naggar (2008) suggested torque readings at depth intervals of 0.3 m along the pile installation and used the average torque in the last 1 m for K_t factor. Sakr (2011a) measured

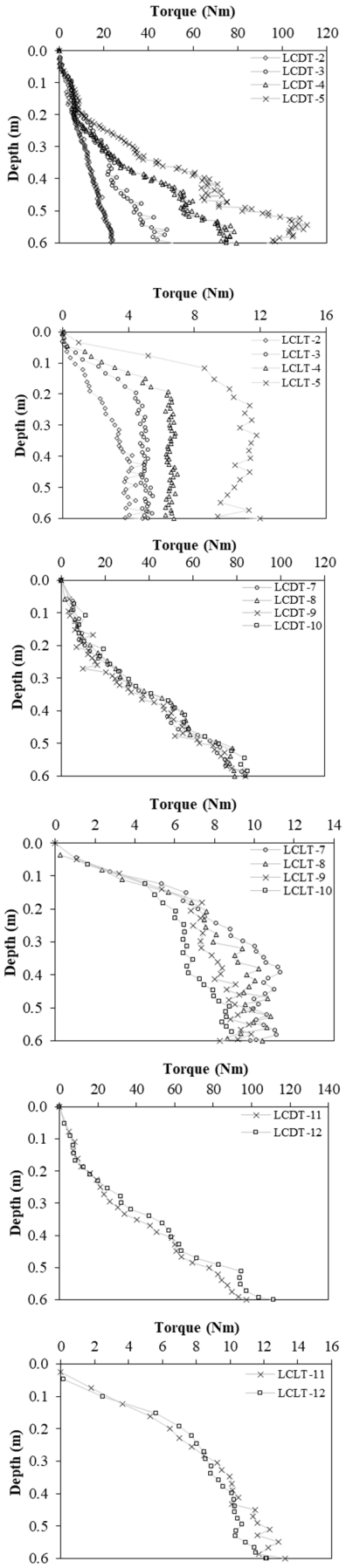

Fig. 4 Measured depth-torque profiles

Table 3 The installation torque measurements

Test ID	$T_{avg.-3d}$ (Nm)	$T_{max.}$ (Nm)	$T_{end\ pile}$ (Nm)
LCDT-2	22.814	23.950	23.150
LCDT-3	43.555	51.140	51.140
LCDT-4	73.973	79.400	79.400
LCDT-5	102.947	110.950	93.110
LCDT-7	78.410	85.550	83.880
LCDT-8	78.220	80.790	79.150
LCDT-9	77.483	83.900	83.900
LCDT-10	81.364	84.970	81.220
LCDT-11	88.475	97.210	97.210
LCDT-12	99.265	111.240	111.240
LCLT-2	4.291	5.210	4.880
LCLT-3	5.129	5.490	5.210
LCLT-4	6.481	6.960	6.780
LCLT-5	10.440	12.010	12.010
LCLT-7	10.523	11.310	9.820
LCLT-8	9.972	11.080	10.420
LCLT-9	9.203	9.890	8.270
LCLT-10	8.471	8.960	7.560
LCLT-11	12.431	13.940	13.240
LCLT-12	11.378	12.190	12.160

torque values at different depths throughout the depth and used maximum torque values for asses the pile ultimate capacities with K_t factor. Tsuha *et al.* (2016) recorded torque readings every 50 cm along installation phase, and the final installation (pile end) torques used to for K_t. Harnish and El Naggar (2017) utilized to establish the K_t factors the average torque over the last installed depth equal to 3D (where D is helix diameter). Al-Rawabdeh *et al.* (2024) recorded installation torque and depth every five second. They computed six different average torque values corresponding to their respective depths (5-30% of the total installation depth) and used the average torque value of 10% of the total installation depth based on regression analysis. In this study, three different installation torque were taken: average torque value over a distance of three times the shaft diameter (3d) preceding the pile tip ($T_{avg.-3d}$), maximum ($T_{max.}$) and installation torques at the pile end ($T_{end\ pile}$). In Fig. 5, the methods for obtaining installation torque were shown on graphical example. $T_{avg.-3d}$, $T_{max.}$ and $T_{end\ pile}$ torques were presented for all tests under the dense and loose soil conditions in Table 3.

When the depth-torque values were examined, it has been determined that the lowest helix meets the soil resistance to a great extent. The reason for this situation can be explained as the first helix entering the soil progresses by disturbing the soil and the next helix is subjected to less soil resistance. For example, in the single-helix LCDT 4, the average installation torque was 73.97 Nm, while the number of helixes doubled (LCDT 7); the average installation torque was 78.41 Nm and the average installation torque was 88.48 Nm in the LCDT 11, where it tripled.

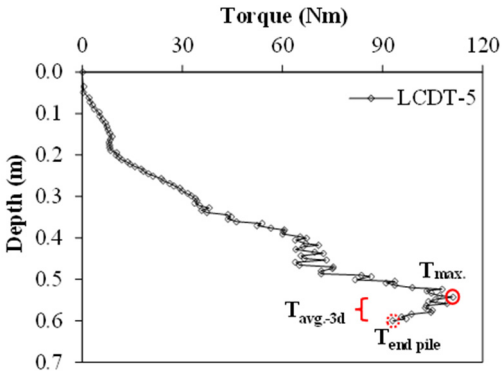

Fig. 5 Determination methods of installation torque

This study advocates for using the average torque over the final three shaft diameters of embedment ($T_{avg.-3d}$) as the most dependable criterion for selecting the design installation torque for helical piles. Maximum torque ($T_{max.}$) is susceptible to being skewed by instantaneous spikes caused by localized soil heterogeneities, which can lead to an overestimation of the pile's bearing capacity. Conversely, the final torque at the pile tip ($T_{end\ pile}$) risks underestimating the true capacity, as it may fail to capture the resistance from more competent soil layers situated just above the tip, particularly if the pile terminates in a soft stratum. $T_{avg.-3d}$ approach effectively reconciles these opposing issues by delivering a more stable and integrated measure of composite soil resistance. This method neutralizes the impact of transient peaks and termination anomalies by averaging the torque across a specified final interval, thereby yielding a more robust and pragmatically sound value for engineering.

3.3 Axial compression tests

Axial compression loading was performed on model helical piles for dense and loose sand soil conditions. The loading-unloading curves for tested at two soil conditions test piles with different helical diameters, double helix with different s/D ratios, and three helix were presented respectively in Fig. 6.

When the load-displacement curves in Fig. 6 were investigated (LCDT-LCLT 2-5), it can be seen that the load values for both soil densities increased significantly with the increase of the helix diameter. When the load-displacement curves of double helix piles were examined in Fig. 6 (LCDT-LCLT 7-10), it is clear that the change of the helix spacing (s) for both density soil does not affect the bearing capacity much, the curves showed that with double helixes piles had almost similar performance.

Similarly, when the load-displacement curves of tri-helix piles that the increase in inter-helix distance ratio (s/D) from 1.5 to 2 are evaluated in Fig. 6 (LCDT-LCLT 11-12), the curves showed almost similar performances for both under loose and dense sand conditions. This can be explained by the effect of the distance between helices in multi-helix piles of relatively shallow conditions (approximately embedment pile length / helix diameter (L/D) ≤ 5).

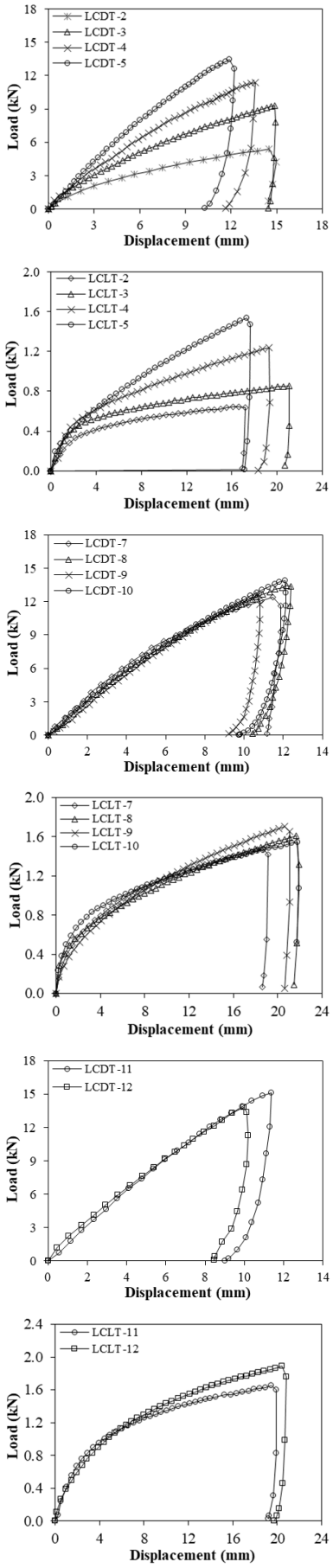

Fig. 6 Load-displacement curves for model test piles

Table 4 Ultimate loads according to failure criteria

Test ID	5%D (kN)	8%D (kN)	10%D (kN)	Davisson (kN)
LCDT-2	2.066	2.792	3.217	2.618
LCDT-3	3.765	5.362	6.206	4.092
LCDT-4	5.397	7.986	9.325	5.047
LCDT-5	7.939	11.611	13.522	6.632
LCDT-7	7.589	10.276	11.566	7.083
LCDT-8	7.013	10.253	11.876	6.629
LCDT-9	6.735	10.142	12.007	6.320
LCDT-10	7.042	10.389	12.201	6.678
LCDT-11	7.756	11.889	13.961	7.336
LCDT-12	7.930	11.715	13.819	7.500
LCLT-2	0.377	0.443	0.478	0.424
LCLT-3	0.532	0.605	0.644	0.551
LCLT-4	0.673	0.818	0.902	0.654
LCLT-5	0.796	1.058	1.219	0.699
LCLT-7	0.878	1.084	1.185	0.847
LCLT-8	0.838	1.023	1.136	0.808
LCLT-9	0.828	1.058	1.192	0.793
LCLT-10	0.946	1.096	1.182	0.922
LCLT-11	1.051	1.250	1.349	1.021
LCLT-12	1.036	1.299	1.432	0.992

3.4 Failure criteria – axial compressive capacity relationship

The ultimate load capacities of helical piles can be obtained with the load-displacement curves obtained from experimental results (International Code Council 2009). In order to interpret the ultimate load values of piles, there are many failure criteria such as the Davisson failure criterion, the Brinch Hansen method, the L_1-L_2 method, the FHWA (5%) method and the ISSMFE (10%) method from the load-displacement curves of the pile loading test results.

In FHWA (5%) method, the load value corresponding to the displacement of 5% of the pile tip diameter is defined as the final axial compression capacity (Sakr 2009, Elsherbiny and El Naggar 2013, Li *et al.* 2018, Bak *et al.* 2021). The tip diameter is taken equal to the diameter of the helical plate in the helical piles and the shaft diameter in the driven piles (O'Neil and Reese 1999). ISSMFE (10%) method that expresses the load amount corresponding to the displacement value corresponding to 10% of the pile diameter as the ultimate pile capacity (George *et al.* 2019, Li and Deng 2019, Bak *et al.* 2021). It is stated that this method overestimates the ultimate capacity of large diameter piles and some pile types (Sakr 2011a). Davisson failure criteria are mainly for driven piles tested according to fast loading methods. It is a method that allows the predetermination of the maximum allowable movement, which takes into account the allowable load value versus the length and size of the pile. The ultimate load capacity is directly dependent on the total displacement, i.e., elastic deflections of the pile and the sum of the offset. 8%D method has been offered for small diameter helices and thin helical piles (Elkasabgy and El Naggar 2014). In this method, the ultimate load value is defined as the load value

Table 5 Different installation torques and K_t relationships

Test ID	Ultimate Capacity (kN)	$T_{(avg.-3d)}$		$T_{(max.)}$		$T_{(end\ pile)}$	
		Torque (Nm)	K_t (m^{-1})	Torque (Nm)	K_t (m^{-1})	Torque (Nm)	K_t (m^{-1})
LCDT-2	2.066	22.814	90.559	23.950	86.263	23.150	89.244
LCDT-3	3.765	43.555	86.442	51.140	73.621	51.140	73.621
LCDT-4	5.397	73.973	72.959	79.400	67.972	79.400	67.972
LCDT-5	7.939	102.947	77.117	110.950	71.555	93.110	85.265
LCDT-7	7.589	78.410	96.786	85.550	88.708	83.880	90.474
LCDT-8	7.013	78.220	89.657	80.790	86.805	79.150	88.604
LCDT-9	6.735	77.483	86.922	83.900	80.274	83.900	80.274
LCDT-10	7.042	81.364	86.549	84.970	82.876	81.220	86.703
LCDT-11	7.756	88.475	87.663	97.210	79.786	97.210	79.786
LCDT-12	7.930	99.265	79.887	111.240	71.287	111.240	71.287
LCLT-2	0.377	4.291	87.868	5.210	72.361	4.880	77.254
LCLT-3	0.532	5.129	103.715	5.490	96.903	5.210	102.111
LCLT-4	0.673	6.481	103.839	6.960	96.695	6.780	99.263
LCLT-5	0.796	10.440	76.243	12.010	66.278	12.010	66.278
LCLT-7	0.878	10.523	83.437	11.310	77.630	9.820	89.409
LCLT-8	0.838	9.972	84.036	11.080	75.632	10.420	80.422
LCLT-9	0.828	9.203	89.975	9.890	83.721	8.270	100.121
LCLT-10	0.946	8.471	111.671	8.960	105.580	7.560	125.132
LCLT-11	1.051	12.431	84.546	13.940	75.395	13.240	79.381
LCLT-12	1.036	11.378	91.053	12.190	84.988	12.160	85.197

(Note: Ultimate capacities were determined 5%D failure criteria)

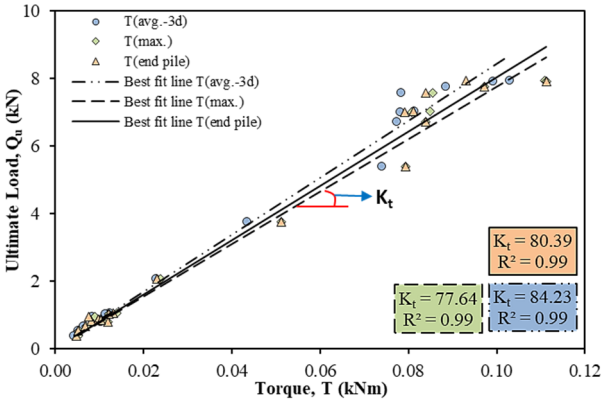

Fig. 7 K_t values for different installation torques

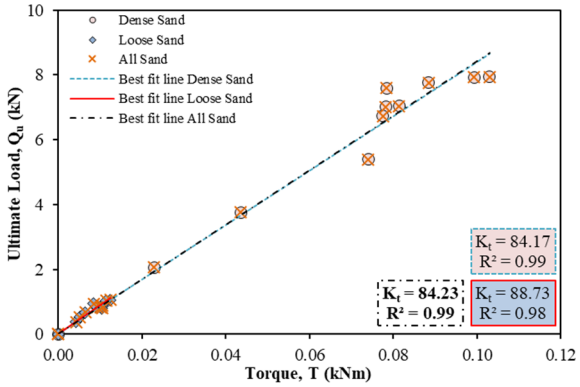

Fig. 8 K_t values for different soil conditions

corresponding to the pile head movement, exceeding the elastic pressure of the pile with 8% of the largest helix diameter capacity (Elkasabgy and El Naggar 2014, El Sharnouby and El Naggar 2012). In this study, FHWA (5%), ISSMFE (10%), 8%D Livneh and El Naggar (2008) and Davisson (1972) failure criteria methods, which are frequently used in helical pile studies under axial compression, were used to find the ultimate pile capacity from load-displacement curves. The ultimate compression capacity estimations are presented in Table 4.

3.5 Installation torque – pile capacity relationship

Three different installation torques were selected to examine the effect of the lack of a standard method of installation torque determination used for the torque-ultimate capacity relationship in the literature on the torque factor K_t. Torque factor K_t values obtained from three installation torque values ($T_{avg.-3d}$, $T_{max.}$ and $T_{end\ pile}$) are presented in Table 5.

In order to examine the effect of the choice of different installation torque ($T_{avg.-3d}$, $T_{max.}$ and $T_{end\ pile}$) on the K_t

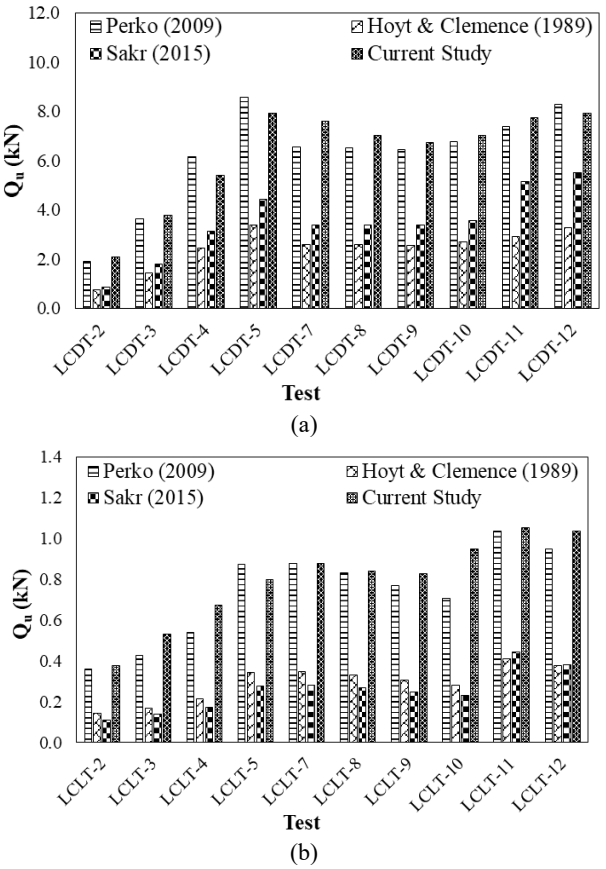

Fig. 9 Ultimate load capacities (a) dense sand and (b) loose sand

value, a linear regression was applied to the graph of the installation torque (Fig. 7). The slope of the trend line passing through zero represents the torque factor K_t. In terms of design, a trend line passing through zero has been proposed (Livneh and El Naggar 2008).

The K_t values expressed the slopes of the best-fit lines determined for $T_{avg.-3d}$, $T_{max.}$ and $T_{end\ pile}$ were calculated as 84.23, 77.64, and 80.39 respectively, and the coefficient of determination of these lines was found as 0.99. It is seen that the lack of a standard for determining the installation torque affects the results. From Fig. 5, it can be seen that the selection of the installation torque can affect the torque factor (K_t) by approximately 10%. Fig. 8 presents the relationship between torque average three times shaft diameter ($T_{avg.-3d}$) and ultimate load capacity (5% failure criteria) and torque factor (K_t) values obtained from this relationship.

Correlation for dense and loose sand conditions tests provided value of K_t equal to 84.17 and 88.73 with coefficients of determination of 0.99 and 0.98, respectively. For all soil type conditions and test modes provided torque factor K_t equal to 84.23 with a coefficient of determination of 0.99. According to the K_t values provided by dense and loose sand soil, it is seen that the soil strength parameter affects the torque factor K_t. The ultimate loads for loose and dense soils were calculated by multiplying installation torques ($T_{avg.-3d}$) with the values of three different torque factors K_t (Hoyt and Clemence 1989, Perko 2009, Sakr 2015) suggested in the literature. The ultimate load values obtained by using these torque factors and determined with 5% were given in Fig. 9 for dense and loose sand soil. As seen the ultimate load obtained using the K_t value suggested by Perko (2009) was given the values closest to the ultimate loads determined from the experimental results, both for dense and loose sands.

The success of a predictive model or statistical analysis is evaluated using key metrics such as the root-mean-square error (RMSE), mean absolute percentage error (MAPE), coefficient of determination (R^2), where lower RMSE and MAPE values and higher R^2 value indicate a better model performance (Mahmoodzadeh *et al.* 2022, Balagosa *et al.* 2024, Samadi *et al.* 2024, Jahangiri *et al.* 2025). To quantitatively assess the predictive accuracy of each method, the mean absolute percentage error (MAPE) was calculated against the experimental data. For the dense sand condition, the analysis revealed that the K_t value proposed by Perko (2009) yielded a MAPE of 7.16%, indicating a high degree of accuracy. In contrast, the methods by Hoyt and Clemence (1989) and Sakr (2015) resulted in significantly higher deviations, with MAPE values of 61.14% and 46.84%, respectively. A similar trend was observed for the loose sand condition, where the Perko (2009) method remained the most accurate with a MAPE of 9.67%, while the approaches of Hoyt and Clemence (1989) and Sakr (2015) produced considerably larger errors of 63.51% and 68.76%. These measurable results furnish robust statistical support for the observations in Fig. 9, confirming that the torque factor suggested by Perko (2009) offers the most reliable predictions for the soil conditions investigated in this study.

3.6 Proposed new equations for torque factor for axially compression loaded helical piles

Souissi (2019) stated that the torque factor associated with the installation torque-pile capacity depends on the shaft diameter only. Harnish and El Naggar (2017) expressed that the K_t value used in establishing the torque-capacity correlation is generally related to the shaft diameter but there are also factors such as helix diameter, installation depth and number of helices, as defined the total embedment area. The embedment area of a helical pile is quantified by the summation of the total net helical area and the lateral surface area of the pile shaft. The net helical area is derived by subtracting the cross-sectional area of the pile shaft from the cumulative gross area of all helices. The lateral surface area of the shaft pertains to the total surface of the pile body that is in contact with the surrounding soil. The geometry of the shaft—whether circular or square—is taken into consideration in the computation of both components, and their final aggregation yields the total embedment area, which represents the complete interaction surface between the pile and the soil. For this reason, there are a number of mathematical expressions in the literature derived based on the correlation relationship between shaft diameter-torque factor (Hoyt and Clemence 1989, Perko 2009) and the embedded area-torque factor (Harnish and El Naggar 2017, Al Rawabdeh *et al.* 2024).

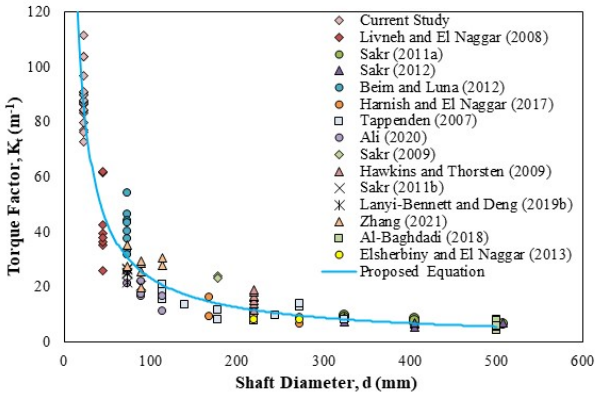

Fig. 10 Torque factor vs shaft diameter

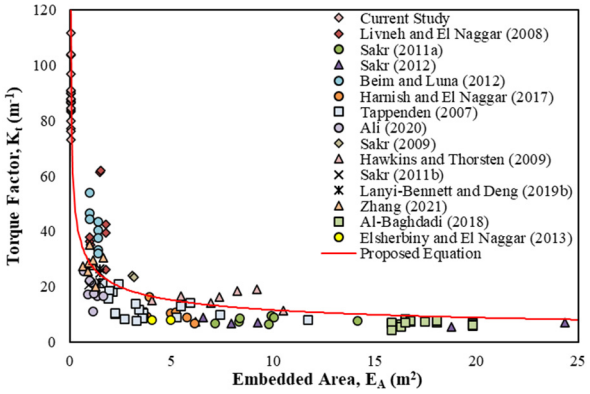

Fig. 11 Torque factor vs embedded area

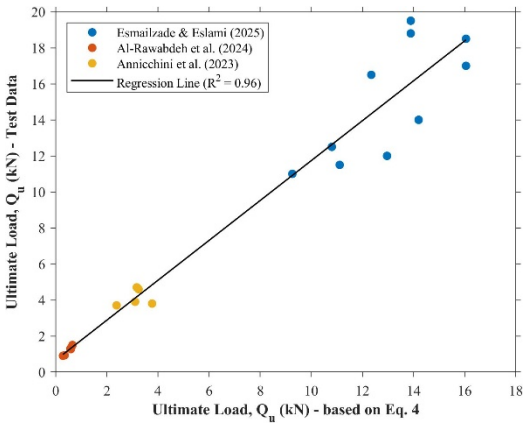

(a)

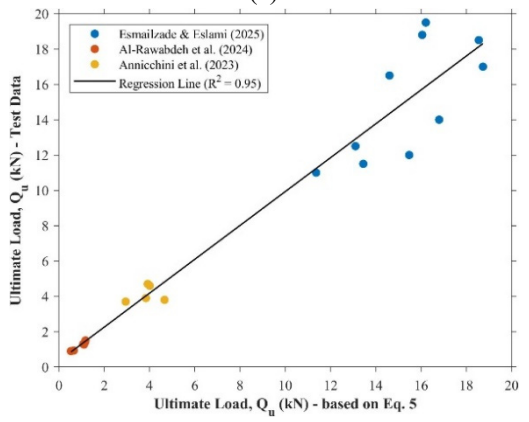

(b)

Fig. 12 Validation of Eqs. 4 (a) and 5 (b) against the test data

In this study, a new database has been created consisting of some laboratory and field test results in the literature and all test results presented current study for the helical piles subjected to axial compression load. The chosen literature studies have test data of various soil types and strength parameters, number of helix, shapes of shaft, installation depths, and helix and shaft diameters. These collected data were obtained from the only compression loading model tests and field load tests. All data presented as 'Current Study' were related with axial compression loadings and selected K_t values were obtained from the ratio of the ultimate capacity determined with 5% failure criteria and average torque over the last installed depth equal to 3d ($T_{avg.-3d}$).

The database assembled for this investigation contains shaft diameter, embedded area, and torque factor values for each helical pile. To explore the correlations between these variables, two primary datasets were analyzed: shaft diameter versus torque factor, and embedded area versus torque factor. These relationships were plotted graphically, and novel mathematical equations were subsequently formulated to define the optimal best-fit curves for each pairing. All curve-fitting procedures were executed using MATLAB (2024), revealing that power functions offered the most suitable regression model for both datasets. These functions were derived by employing the nonlinear least-squares method, specifically utilizing the trust-region-reflective algorithm. As an illustration, Fig. 10 presents the graphical relationship derived from the torque factor (K_t) versus shaft diameter (d) series, with the resulting empirical equation presented in Eq. (4).

$$K_t = 1339d^{-0.88} \quad (4)$$

As seen the statistical correlation based on compression test results and shaft diameter has very strong correlations (R^2=0.94). The proposed equation (in Eq. (4)) is recommended to be used as an alternative to the functions in the literature for the calculation torque factor depending on the shaft diameter. The torque factor (K_t) versus embedded area (E_A) series from the database were shared as a graph in Fig. 11 and the novel proposed equation was given in Eq. (5).

$$K_t = 28.4{E_A}^{-0.39} \quad (5)$$

The curve appears to represent the data points quite well, with a good relationship performance (R^2=0.90). The equation proposed in Eq. (5) stands out as a more reasonable expression in which additional helical pile parameters were also considered as an alternative to a torque factor correlation that depends only on the shaft diameter.

In this study, 95% confidence intervals were calculated to assess the statistical significance of the model coefficients and the precision of the forecasts obtained

through nonlinear regression. The analysis was fundamentally based on the power function $y=ax^b$ which provides the most ideal outcomes for curve fitting. For the model detailed in Eq. (4), the 95% confidence interval for coefficient a was found to be (1105, 1573), whereas for the exponent b, this range was calculated as (−0.93, −0.83). The intervals for the model in Eq. (5) were determined as (26.34, 30.43) for coefficient a and (−0.42, −0.36) for b. Critically, for both models proposed in Eqs. (4) and (5), the fact that these confidence intervals do not contain zero confirms the statistical significance of the estimated coefficients and supports the robustness of the models' fit to the data.

To determine the ultimate load, the torque factors proposed in Eqs. (4) and (5) were benchmarked against findings from existing literature. For validation, an independent experimental dataset was compiled, amounting to approximately 20% of the model data shown in Figs. 10 and 11. The outcomes of this validation process were illustrated in Fig. 12.

The fact that the coefficients of determination of the functions presented in Eqs. (4) and (5) were very great shows that the torque factors shared in the literature and obtained in this study were highly compatible with the proposed equations. Since determining the torque factor based on shaft diameter is widely and traditionally preferred in the literature and engineering practices, a function that calculates the K_t value depending on the shaft diameter was shared in Eq. (4). On the other hand, a more realistic solution would be to use the embedded area-based torque factor function presented in this study (Eq. (5)), to determine K_t value of helical piles in empirically. Therefore to find the torque factor, a more realistic approach (Eq. (5)) depending on the embedded area was presented compared to based only on shaft diameter, by taking into account the helix diameter, shaft shape, installation depth, and number of helices. This function based on the embedded area-torque factor given in Eq. (5) can represent the K_t change very consistently, especially in helical piles where the shaft diameter is constant but with different helix number and diameter.

4. Conclusions

This investigation presents an experimental appraisal of model helical pile tests. During the pile installation process, torque values were recorded throughout the depth and the obtained findings have been evaluated by the capacity-torque relationship. Integrating test results into an exhaustive multi-scale database to establish novel and robust torque correlation factor equations for compression-loaded helical piles. The key conclusions derived from the experimental and analytical work are as follows:

• Based on the non-linear regression of this broad dataset, a new formulation $\boldsymbol{K_t = 1339d^{-0.88}}$ solely dependent on shaft diameter was set. The high coefficient of determination (R^2=0.94) across this wide dimensional spectrum validates this equation as a generalized tool. This methodological framework, leveraging heterogeneous data, empirically bridges the gap between laboratory and field scales, thus enabling the prediction of the torque correlation coefficient for varying shaft diameters.

• A more physically comprehensive expression was advanced, put forth in the article as a second novel relationship $\boldsymbol{K_t = 28.4E_A^{-0.39}}$ correlating torque factor with the total embedded area (E_A). K_t-based on E_A incorporates the contribution of more design parameters, such as shaft diameter, helix diameters, embedment depth, and number of helices. This formulation also showed a strong dependence (R^2=0.90) and is recommended as a more holistic approach for accurately predicting torque correlation factor.

• Although the embedded area (E_A) based model results in a marginal reduction in the determination coefficient compared to the shaft diameter (d) based model, this trade-off is significantly justified by the formulation's superior physical grounding and its holistic integration of multiple critical design parameters.

• Perko (2009) approach was found to provide the ultimate load predictions closest to the ultimate compressive loads determined by 5%D method for the model tests in this research. In contrast, the suggestions by Hoyt and Clemence (1989) and Sakr (2015) yielded less proximate results for the configurations tested in this paper. This finding strongly supports the study's focused approach on treating shaft diameter—and as a more comprehensive proposal, the embedded area—as the primary correlation parameters.

• The torque factor (K_t) was shown to be sensitive to soil conditions, with experimentally derived values of 88.73 m^{-1} for loose sand and 84.17 m^{-1} for dense sand (with R^2 approx. 0.99), confirming the influence of soil strength parameters on the torque-capacity relationship.

• In the correlations established in this paper, the definition of the installation torque ($T_{avg\text{-}3d}$, T_{max}, T_{end}) was found to impact the resulting K_t value by approximately 10%, highlighting the importance of selecting the torque read method. Furthermore, this article adopts the use of the average torque approach as a safer strategy for determining the installation torque.

Acknowledgments

The work presented in this paper was carried out with funding from TUBITAK (The Scientific and Technological Research Council of Turkey) grant number 218M571. The second author is supported by TÜBİTAK (The Scientific and Technological Research Council of Turkey) BİDEB 2211-A National Scholarship Program, and YÖK (The Council of Higher Education) 100/2000 Ph.D. Scholarship Project.

References

Al-Baghdadi, T. (2018), “Screw piles as offshore foundations: numerical and physical modelling”, Ph.D. Dissertation,

University of Dundee, Dundee.
Ali M. (2020), "Field axial loading testing of helical piles at a cohesionless soil site", M.Sc. Thesis, The University of Alberta, Alberta. https://doi.org/10.7939/r3-m5dd-yx25.
Al-Rawabdeh, A.M.A., Vinod, J.S. and Liu and M.D. (2024), "Large-scale laboratory testing of helical piles: Effect of the shape", *Geotech. Geol. Eng.*, **42**, 1675-1692. https://doi.org/10.1007/s10706-023-02640-0.
Annicchini, M.M., Schiavon, J.A. and Tsuha, C. (2023), "Effects of installation advancement rate on helical pile helix behavior in very dense sand", *Acta Geotech.*, **18**, 2795-2811. https://doi.org/10.1007/s11440-022-01713-3.
Aoki, N., Tsuha, C.H.C., Thorel, L., Rault, G. and Garnier, J. (2007), "Physical modelling of helical pile anchors", *Int. J. Phys. Model. Geotech.*, **7**. https://doi.org/10.1680/ijpmg.2007.7.4.01.
Asgari, A., Arjomand, M.A., Bagheri, M., Ebadi-Jamkhaneh, M. and Mostafaei, Y. (2025), "Assessment of experimental data and analytical method of helical pile capacity under tension and compressive loading in dense sand", *Build.*, **15**(15), 2683. https://doi.org/10.3390/buildings15152683.
ASTM D2167-15 (2015), Standard Test Method for Density and Unit Weight of Soil in Place by the Rubber Balloon Method. ASTM International, West Conshohocken, PA, 2015, www.astm.org.
ASTM D2487-11 (2011), Standard Practice for Classification of Soils for Engineering Purposes (Unified Soil Classification System). ASTM International, West Conshohocken, PA, 2011, www.astm.org.
ASTM D4253-16e1 (2016), Standard Test Methods for Maximum Index Density and Unit Weight of Soils Using a Vibratory Table. ASTM International, West Conshohocken, PA, 2016, www.astm.org.
ASTM D4254-16 (2016), Standard Test Methods for Minimum Index Density and Unit Weight of Soils and Calculation of Relative Density. ASTM International, West Conshohocken, PA, 2016, www.astm.org
Bak, H.M., Halabian, A.M., Hashemolhosseini, H., Rowshanzamir and M. (2021), "Axial response and material efficiency of tapered helical piles", *J. Rock Mech. Geotech. Eng.*, **13**. https://doi.org/10.1016/j.jrmge.2020.04.007.
Balagosa, J.A., Lee, M.J., Choo, Y.W., Kim, H.S. and Kim, J.M. (2024), "Effect of wood pellet fly ash on strength and microstructure of Korean weathered granite soil", *Geomech. Eng.*, **38**(4), 335-352. https://doi.org/10.12989/gae.2024.38.4.335.
Beim, J. and Luna, S.C. (2012), "Results of dynamic and static load tests on helical piles in the varved clay of Massachusetts", *DFI J.*, **6**(1), 58-67. https://doi.org/10.1179/dfi.2012.005.
CFEM. (2006), "Canadian Foundation Engineering Manual", 4th Ed., The Canadian Geotechnical Society, BiTech Publishers Ltd.
Davisson, M.T. (1972), "High Capacity Piles", Proceedings of Lecture Series on Innovations in Foundation Construction, ASCE, Illinois Section, Chicago, 81-112.
Ebadi-Jamkhaneh, M., Arjomand, M.A., Bagheri, M., Asgari, A., Nouhi Hefzabad, P., Salahi, S. and Mostafaei, Y. (2025), "Experimental study on the pullout behavior of helical piles in geogrid-reinforced dense shahriyar sand", *Build.*, **15**(16), 2963. https://doi.org/10.3390/buildings15162963
El Sharnouby, M.M. and El Naggar, M.H. (2012), "Field investigation of axial monotonic and cyclic performance of reinforced helical pulldown micropiles", *Can. Geotech. J.*, **49**(5), 560-573. https://doi:10.1139/t2012-017.
Elkasabgy, M. and El Naggar, M.H. (2014), "Axial compressive response of large-capacity helical and driven steel piles in cohesive soil", *Can. Geotech. J.*, **52**. https://doi.org/10.1139/cgj-2012-0331.
Elsherbiny, Z.H. and El Naggar, M.H. (2013), "Axial compressive capacity of helical piles from field tests and numerical study", *Can. Geotech. J.*, **50**. https://doi.org/10.1139/cgj-2012-0487.
Esmailzade, M. and Eslami, A. (2025), "Experimental study on performance and enhanced methods of helical piles using Frustum Confining Vessel in Anzali Sand", *Ocean Eng.*, **324**, 120624. https://doi.org/10.1016/j.oceaneng.2025.120624.
Fateh, A.M.A., Eslami, A. and Fahimifar, A. (2018), "A study of the axial load behaviour of helical piles in sand by frustum confining vessel", *Int. J. Phys. Model. Geotech.*, **18**. https://doi.org/10.1680/jphmg.16.00007.
Gavin, K., Doherty, P. and Tolooiyan, A. (2014), "Field investigation of the axial resistance of helical piles in dense sand", *Can. Geotech. J.*, **51**. https://doi.org/10.1139/cgj-2012-0463.
George, B.E., Banerjee, S. and Gandhi, S.R. (2019), "Helical piles installed in cohesionless soil by displacement method", *Int. J. Geomech.*, **19**. https://doi.org/10.1061/(asce)gm.1943-5622.0001457.
Harnish, J.L. (2015), "Helical pile installation torque and capacity correlations", Ph.D. Dissertation, The University of Western Ontario.
Harnish, J.L. and El Naggar, M.H. (2017), "Large-diameter helical pile capacity – torque correlations", *Can. Geotech. J.*, **54**. https://doi.org/10.1139/cgj-2016-0156.
Hawkins, K. and Thorsten, R. (2009), "Load test results—Large diameter helical pipe piles", *Contemporary Topics in Deep Foundations*, 488-495. https://doi.org/10.1061/41021(335)61.
Hoyt, R.M. and Clemence, S.P. (1989), "Uplift capacity of helical anchors in soil", *Proceedings of the 12th International Conference on Soil Mechanics and Foundation Engineering*, ISSMFE, Rio de Janeiro.
International Code Council. (2009), International Building Code (IBC). International Code Council, Washington, DC.
Jahangiri, V., Akbarzadeh, M.R., Shahamat, S.A., Asgari, A., Naeim, B. and Ranjbar, F. (2025), "Machine learning-based prediction of seismic response of steel diagrid systems", *Struc.*, **80**, 109791. https://doi.org/10.1016/j.istruc.2025.109791.
Kim, H.J., Reyes, J.V., Dinoy, P.R., Park, T.W., Kim, H.S. and Kim, J.Y. (2022), "Modified p-y curves to characterize the lateral behavior of helical piles", *Geomech. Eng.*, **31**(5), 505-518. https://doi.org/10.12989/gae.2022.31.5.505.
Kim, H.J., Kim, H.S., Dinoy, P.R., Reyes, J.V., Jeong, Y.S., Park, J.Y. and Mawuntu, K.B.A. (2023), "Estimating the lateral profile of helical piles using modified p-y springs", *Geomech. Eng.*, **35**(1), 1-11. https://doi.org/10.12989/gae.2023.35.1.001.
Kishida, H. (1963), "Stress distribution of model piles in sand", *Soils Found.*, **4**(1), 1-23. https://doi.org/10.3208/sandf1960.4.1.
Lanyi-Bennett, S.A. and Deng, L. (2019a), "Axial load testing of helical pile groups in glaciolacustrine clay", *Can. Geotech. J.*, **56**. https://doi.org/10.1139/cgj-2017-0425.
Lanyi-Bennett, S.A. and Deng, L. (2019b), "Effects of inter-helix spacing and short-term soil setup on the behaviour of axially loaded helical piles in cohesive soil", *Soils Found.*, **59**(2), 337-350. https://doi.org/10.1016/j.sandf.2018.12.002.
Li, W. and Deng, L. (2019), "Axial load tests and numerical modeling of single-helix piles in cohesive and cohesionless soils", *Acta Geotech.*, **14**. https://doi.org/10.1007/s11440-018-0669-y.
Li, W., Zhang, D.J.Y., Sego, D.C. and Deng, L. (2018), "Field testing of axial performance of large-diameter helical piles at two soil sites", *J. Geotech. Geoenviron. Eng.*, **144**. https://doi.org/10.1061/(asce)gt.1943-5606.0001840.
Livneh, B. and El Naggar, M.H. (2008), "Axial testing and numerical modeling of square shaft helical piles under compressive and tensile loading", *Can. Geotech. J.*, **45**. https://doi.org/10.1139/T08-044.

Lutenegger, A.J. and Tsuha, C.H.C. (2015), "Evaluating installation disturbance from helical piles and anchors using compression and tension tests", *Proceedings of the 15th Pan-American Conference on Soil Mechanics and Geotechnical Engineering*.

Mahmoodzadeh, A., Taghizadeh, M., Mohammed, A.H., Ibrahim, H.H., Samadi, H., Mohammadi, M. and Rashidi, S. (2022), "Tunnel wall convergence prediction using optimized LSTM deep neural network", *Geomech. Eng.*, **31**(6), 545-556. https://doi.org/10.12989/gae.2022.31.6.545.

MATLAB (2024), MATLAB program version: 9.10.0 (R2021a), Natick, Massachusetts: The MathWorks Inc.

O'Neil, M.W. and Reese, L.C. (1999), Drilled shafts: Construction procedures and design methods; FHWA: Washington D.C, USA.

Perko, H.A. (2009), "Helical piles: A practical guide to design and installation", John Wiley & Sons, Ltd. https://doi.org/10.1002/9780470549063.

Sahil, A.W., Uchimura, T., Malik, A.A. and Kabir, M.R. (2025), "A comparative study on the end-bearing capacity of toe-wing & spiral screw piles in cohesionless soil", *Build.*, **15**(4), 525. https://doi.org/10.3390/buildings15040525.

Sakr, M. (2009), "Performance of helical piles in oil sand", *Can. Geotech. J.*, **46**. https://doi.org/10.1139/T09-044.

Sakr, M. (2011a), "Installation and performance characteristics of high capacity helical piles in cohesionless soils", *DFI J.*, **5**. https://doi.org/10.1179/dfi.2011.004.

Sakr, M. (2011b), "Helical piles-An effective foundation system for solar plants", *Proceedings of The 64th Canadian Geotechnical Conference and Pan-AM CGS*, Ontario.

Sakr, M. (2012), "Installation and performance characteristics of high capacity helical piles in cohesive soils", *DFI J.*, **6**(1), 41-57. https://doi.org/10.1179/dfi.2012.004.

Sakr, M. (2015), "Relationship between installation torque and axial capacities of helical piles in cohesionless soils", (retracted), *J. Perform. Constr. Fac.*, **29**. https://doi.org/10.1061/(asce)cf.1943-5509.0000621.

Salhi, L., Nait-Rabah, O., Deyrat, C. and Roos, C. (2013), "Numerical modeling of single helical pile behavior under compressive loading in sand", *Electron. J. Geotech. Eng.*, **18**.

Samadi, H., Alanazi, A., Muhodir, S. H., Alsubai, S., Alqahtani, A. and Marzougui, M. (2024), "In-depth exploration of machine learning algorithms for predicting sidewall displacement in underground caverns", *Geomech. Eng.*, **37**(4), 307-321. https://doi.org/10.12989/gae.2024.37.4.307.

Souissi, M. (2019), "Helical pile capacity to torque ratio: A functional perspective", Ph.D. Dissertation, Colorado State University, USA.

Souissi, M. (2020), "Helical pile capacity-to-torque correlation: A more reliable capacity-to-torque factor based on full scale load tests", *DFI J.*, **14**. https://doi.org/10.37308/dfijnl.20190716.208.

Sprince, A. and Pakrastinsh, L. (2010), "Helical pile behaviour and load transfer mechanism in different soils", *Proceedings of the 10th International Conference Modern Building Materials*, Structures and Techniques.

Tappenden, K.M. (2007), "Predicting the axial capacity of screw piles installed in western Canadian soils", M.Sc. Thesis, The University of Alberta, Alberta. https://doi.org/10.7939/R3SX64K96.

Tsuha, C.H.C., dos Santos Filho, J.M.S.M. and da Costa Santos, T. (2016), "Helical piles in unsaturated structured soil: A case study", *Can. Geotech. J.*, **53**. https://doi.org/10.1139/cgj-2015-0017

Türedi, Y. and Örnek, M. (2020), "Analysis of model helical piles subjected to axial compression", *Gradevinar*, **72**(9), 759-769. https://doi.org/10.14256/JCE.2660.2019.

Yang, Y., de Lange, D.A., Wang, H. and Askarinejad, A. (2024), "Multi-scale calibration of a line-style sand pluviator", *Geomech. Eng.*, **37**(5), 431-441. https://doi.org/10.12989/gae.2024.37.5.431.

Yu, F. and Yang, J. (2012), "Bearing capacity of open-ended steel pipe piles in sand", *J. Geotech. Geoenviron. Eng.*, **138**(9), 1116-1128. https://doi.org/10.1061/(ASCE)GT.1943-5606.0000667.

Zhang, Y. (2021), "Field testing of helical piles and spt-based method for estimating axial capacities in sand", M.Sc. Thesis, The University of Alberta, Alberta. https://doi.org/10.7939/r3-1hvb-w957

JS